PCCP

PAPER

View Article Online
View Journal | View Issue

Cite this: *Phys. Chem. Chem. Phys.*, 2017, **19**, 14486

Novel magnesium borides and their superconductivity†

M. Mahdi Davari Esfahani,[a] Qiang Zhu,[a] Huafeng Dong,[a] Artem R. Oganov,*[abcd] Shengnan Wang,[a] Maksim S. Rakitin[ae] and Xiang-Feng Zhou[af]

Received 8th February 2017,
Accepted 3rd April 2017

DOI: 10.1039/c7cp00840f

rsc.li/pccp

With the motivation of searching for new superconductors in the Mg–B system, we performed *ab initio* evolutionary searches for all the stable compounds in this binary system in the pressure range of 0–200 GPa. We found previously unknown, yet thermodynamically stable, compositions MgB_3 and Mg_3B_{10}. Experimentally known MgB_2 is stable in the entire pressure range 0–200 GPa, while MgB_7 and MgB_{12} are stable at pressures below 90 GPa and 35 GPa, respectively. We predict a reentrant behavior for MgB_4, which becomes unstable against decomposition into MgB_2 and MgB_7 at 4 GPa and then becomes stable above 61 GPa. We find ubiquity of phases with boron sandwich structures analogous to the AlB_2-type structure. However, with the exception of MgB_2, all other magnesium borides have low electron–phonon coupling constants λ of 0.32–0.39 and are predicted to have T_c below 3 K.

Introduction

Tremendous efforts have been made to design conventional superconductors with higher and higher critical temperatures.[1–5] It is also the main focus of theoretical and experimental studies to determine how high the superconducting transition temperature T_c can be pushed in binary and ternary boron-compounds. For instance, theoretical studies predicted thermodynamically unstable CaB_2 to be superconducting at $\sim$50 K[1] and hole-doped LiBC to have T_c of 65 K.[2] Ternary Mo_2Re_3B with T_c = 8.5 K,[3] $CuB_{2-x}C_x$ ($T_c \sim 50$ K)[4] and the multiple-phase bulk sample of yttrium-palladium-boron-carbon (T_c = 23 K[5]) are important boron-based superconductors.

The unexpected discovery of superconductivity in MgB_2 with high T_c = 39 K[6] has triggered a flurry of publications. In previous studies, superconductivity of MgB_2 has been thoroughly investigated.[7–11] The isotope effect demonstrated the phonon-mediated nature of superconductivity in this compound.[12] Although doping is usually expressed as a hope to enhance the desired properties, carbon-doped MgB_2 ($Mg(B_{0.8}C_{0.2})_2$) has a lower T_c = 21.9 K.[13] Aluminum, with one more electron than magnesium, was reported to be an unfit candidate for partial substitution for magnesium ($Mg_{1-x}Al_xB_2$).[14] This shows that increasing electron concentration suppresses the superconductivity of magnesium diboride.

Elemental magnesium[15] and boron[16] have been shown to exhibit unexpected chemistry under high pressure, raising the motivation of studying their compounds. Moreover, materials composed of light atoms could make good conventional superconductors. The Mg–B system was subjected to some explorations of superconductivity.[17–19] Stability of boron-rich magnesium borides, *e.g.*, MgB_7, MgB_{12} and $Mg_{\sim 5}B_{44}$, has been extensively studied by experiment at ambient pressure.[20] Borides of similar metals, *e.g.*, Ca–B[21] and Li–B,[22] and the stability of 41 metal borides[23] were studied and new compounds were shown to appear at high pressure. The high-pressure phase of MgB_2 (KHg_2-type structure) was reported to be a poor metal with no superconductivity, highlighting the main role of delocalized bonding of the boron honeycomb layers in the superconducting properties of MgB_2 with the AlB_2-type structure.[18]

To date, no comprehensive and systematic theoretical research has been reported on the stability and properties of magnesium borides at high pressure. Here, with the knowledge of the important role of magnesium,[13] the crucial existence of honeycomb boron layers[18] and the substantial effect of electron concentration,[14] we present results of extensive computational searches for stable magnesium borides Mg_xB_y and their superconductivity.

[a] *Department of Geosciences, Center for Materials by Design, and Institute for Advanced Computational Science, State University of New York, Stony Brook, NY 11794-2100, USA. E-mail: artem.oganov@stonybrook.edu*
[b] *Skolkovo Institute of Science and Technology, Skolkovo Innovation Center, 3 Nobel St., Moscow 143026, Russia*
[c] *Moscow Institute of Physics and Technology, 9 Institutskiy Lane, Dolgoprudny City, Moscow Region 141700, Russia*
[d] *International Center for Materials Design, Northwestern Polytechnical University, Xi'an, 710072, China*
[e] *NSLS-II, Brookhaven National Laboratory, Upton, NY 11973-5000, USA*
[f] *School of Physics and Key Laboratory of Weak-Light Nonlinear Photonics, Nankai University, Tianjin 300071, China*

† Electronic supplementary information (ESI) available. See DOI: 10.1039/c7cp00840f

Methods

An *ab initio* variable-composition evolutionary method USPEX[24–27] was applied to the Mg–B system at 0, 30, 50, 75, 100, 150 and 200 GPa. This method has the capability of finding possible compositions and the corresponding stable and metastable structures at given pressures, and successfully predicted new phases of MgB_2 at high pressure[18] and new stable phases of different systems like Na–Cl, boron and Na–He.[16,28,29] High-temperature superconductivity in hydrogen-rich compounds, *e.g.*, Sn–H[30] and Ge–H,[31] was also studied. In this method, we created initial generation of structures and compositions randomly with up to 28 atoms in the primitive cell. Subsequent generations were obtained using heredity, transmutation, softmutation, and a random symmetric generator.[32]

Structure relaxations were carried out using the VASP package[33] in the framework of density functional theory (DFT) adopting PBE-GGA (Perdew–Burke–Ernzerhof generalized gradient approximation).[34] The projector augmented-wave approach (PAW)[35] with the [He] core for both Mg and B atoms was used to describe the core electrons and their effects on valence orbitals. A plane-wave kinetic energy cutoff of 600 eV and dense Monkhorst–Pack *k*-point grids with a reciprocal space resolution of $2\pi \times 0.03$ Å^{-1} were used.[36] Phonon frequencies and electron–phonon coupling (EPC) were calculated using Quantum ESPRESSO.[37] The PBE-GGA functional was used for this part. A plane-wave basis set with a cutoff of 60 Ry gave a convergence in energy with a precision of 1 meV per atom. For electron–phonon coupling, $6 \times 6 \times 2$, $6 \times 6 \times 4$ and $4 \times 4 \times 4$ *q*-point meshes were used for *C*2/*m*-MgB_3, *Amm*2-Mg_3B_{10} and *C*2/*m*-MgB_4, respectively. Denser *k*-point meshes, $12 \times 12 \times 4$, $12 \times 12 \times 8$ and $8 \times 8 \times 8$, were used for the convergence checks of the EPC parameter λ.

Results

Search for stable compounds

Pressure can stabilize new or destabilize the known compounds, and a proper sampling of all promising compositions is needed. In Fig. 1(a), the enthalpies of formation ΔH_f per atom (with respect to the stable structures of elemental magnesium and boron) are shown in the convex hull form as obtained from all possible compounds. The convex hull gives all thermodynamically stable compositions of a multicomponent system, and their enthalpies of formation (per atom). The convex hull (see Fig. 1(a)) includes all thermodynamically stable states, while unstable ones will always appear above it. The distance of an arbitrary compound above the tieline of the convex hull is a measure of its instability, as it shows the decomposition energy of that compound into the nearest stable compounds. The convex hull construction shows that boron-rich compounds are stabilized at high pressure.

Taking our predicted structures/compounds and experimentally known large-cell structures of MgB_7, $Mg_{\sim 5}B_{44}$, MgB_{12} (all three compounds feature B_{12}-icosahedra, and for the latter two, we constructed ordered approximants of disordered experimental structures – for MgB_{12} containing 388 atoms in the unit cell), we computed the phase diagram of the Mg–B system. At pressures studied here, MgB_2, MgB_3, Mg_3B_{10}, MgB_4, MgB_7 and MgB_{12} have stability fields, making the phase diagram (Fig. 1(b)) very rich. A recent list of 41 metal borides presented in ref. 23 at 0 and 30 GPa, clearly demonstrates that metal borides often have a variety of stable phases at high pressure.

Upon increasing pressure metastable compounds, MgB_3 and MgB_6, get closer to the tieline. Our calculations indicate that at 54 GPa, MgB_3 reaches stability and forms the *C*2/*m* structure. Unlike MgB_3, MgB_6 cannot compete with other compounds and remains metastable throughout the entire pressure range (0 to 200 GPa).

Although MgB_6 emerges as a metastable compound from our calculations, we still studied it, keeping in mind recent observation of superconductivity in YB_6.[38] Moreover, there is experimental evidence for MgB_6 as a non-equilibrium phase.[39]

MgB_2

Some of us studied high-pressure phases of MgB_2 using the evolutionary algorithm USPEX.[18] Our results are in good accordance with that study, as the phase transition occurs at 190 GPa. The transition from the AlB_2-type structure (Fig. 2) with the space group *P*6/*mmm* to the KHg_2-type structure with the space group *Imma*, completely destroys superconductivity. The role of the B–B π-bonded network and charge transfer from Mg to B atoms are explained as having major roles in superconducting properties.[11,18]

MgB_3

MgB_3, one of the new high-pressure compounds, lies 5 meV per atom above the MgB_2–MgB_7 tieline at 50 GPa. It becomes stable at 54 GPa and remains stable up to 130 GPa in the *C*2/*m* phase. Finally the *Cmcm* structure becomes more favorable than all other possible structures up to 200 GPa. AB_3 is interestingly a common stoichiometry for metal borides as reported for WB_3,[40] MnB_3[41] and NaB_3;[23] however, MgB_3 has not been studied yet, neither computationally nor experimentally.

MgB_3 stabilizes at high pressure, while CaB_3[21] and LiB_3[22] are not stable even at high pressure. Structural information for the predicted stable MgB_3 phases is provided in Table 2 and in Fig. 3. The metastable layered *C*2/*m* phase at pressures below 43 GPa is important, since it has a graphene-like hexagonal boron pattern, which may be a hint of a potentially superconducting phase.

MgB_4

MgB_4 has a remarkable reentrant behavior: this compound is thermodynamically stable in the pressure range 0–4 GPa, then becomes unstable decomposing into other borides, and then again becomes thermodynamically stable at pressures >61 GPa (Fig. 1(b)). Below we will consider lowest-enthalpy phases corresponding to this composition (see Fig. 4).

The *Pnma* phase of MgB_4 is stable at ambient pressure in accordance with theoretical[23] and experimental[42] results and remains the most favorable phase up to 31 GPa. Unlike all the other MgB_4 phases and most of the magnesium borides under different pressure conditions, which are metallic, *Pnma*–MgB_4 is a semiconductor. The predicted phase diagram shows that at 31 GPa the semiconducting state breaks down, and MgB_4 transforms into a metallic *C*2/*m* (similar to AlB_2-type) structure.

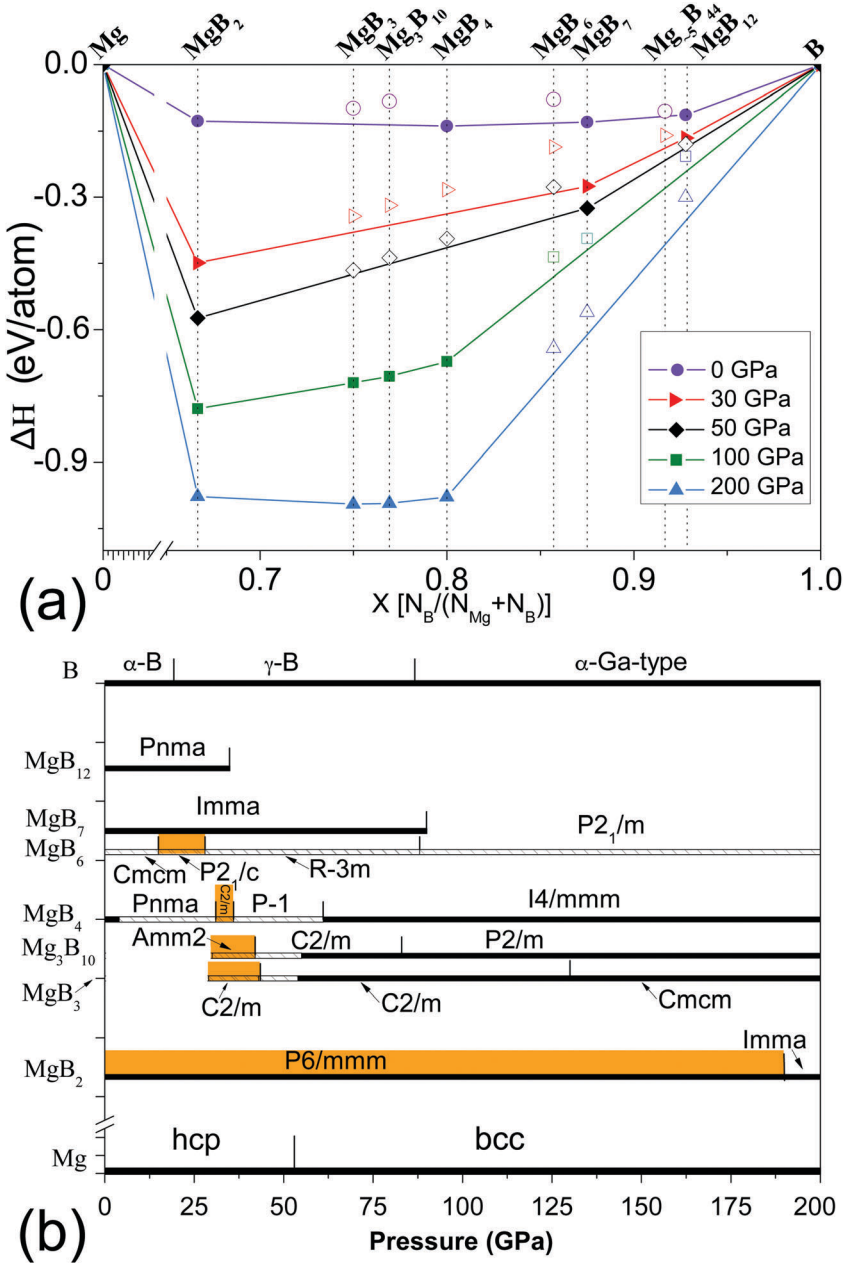

Fig. 1 Stability of magnesium borides. (a) Calculated convex hulls at different pressures. α-phase, γ-phase and α-Ga-type structures are used for boron[16] and for magnesium, hexagonal close-packed (hcp) and body-centered cubic (bcc) structures were used.[15] (b) Pressure-composition phase diagram. Solid bars show stable phases, whereas hatched bars indicate metastability. Colored areas illustrate layered structures (boron sandwiches) analogous to the AlB_2-type structure.

*C*2/*m* has the lowest enthalpy in a narrow pressure range from 31 to 36 GPa. From 36 to 60 GPa, the $P\bar{1}$ phase becomes more favorable, and at very high pressures (60–200 GPa), a high symmetry structure, *I*4/*mmm*, becomes stable.

The main features of *I*4/*mmm* and $P\bar{1}$ phases are prisms of boron atoms that hold one or two magnesium atoms. Having boron double-layers (in comparison with *P*6/*mmm*-MgB_2), the *C*2/*m* structure can be described as a boron sandwich of this composition. Boron sandwiches have graphene-like layer(s) of boron, intercalated by magnesium atoms. Phonon calculations were performed to check the dynamical stability throughout the Brillouin zone. We did not find any dynamical instability (see Fig. 10 and Fig. S9, ESI†). Due to high density of states (DOS) at the Fermi level ($N(E_f)$), high-pressure phases of MgB_4 can be potential candidates for superconductivity. Electron–phonon coupling (EPC) calculations revealed that among MgB_4 phases, only layered *C*2/*m*-MgB_4 is a superconductor.

MgB_4 has analogous stoichiometry to many AB_4 systems, *e.g.* MnB_4,[41,43] CrB_4,[44] CaB_4[45,46] and so forth. AB_4 structures are mostly orthorhombic or tetragonal with 20 atoms per cell. Some of these structures are in the $BaAl_4$-type structure with the space group *I*4/*mmm*.[47] By removing Mg from the prisms, one observes a pattern similar to the α-Ga structure of boron.[16]

By increasing pressure, we see the emergence of a graphene-like boron double-layered phase (MgB_2 has a simple hexagonal

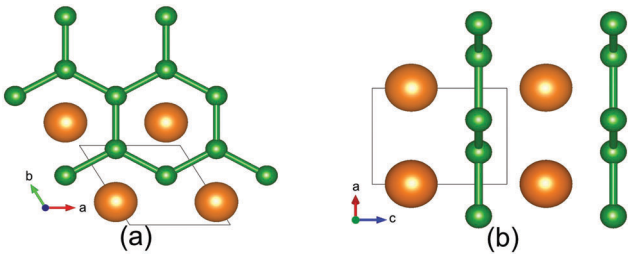

Fig. 2 Structure of a thermodynamically stable MgB_2 phase with the space group *P6/mmm*. Projections of the layered structure along the (a) [001] and (b) [010] directions.

Table 1 Computed superconducting T_c of different sandwich borides

Structure	MgB_2 (*P6/mmm*)	MgB_3 (*C2/m*)	Mg_3B_{10} (*Amm2*)	MgB_4 (*C2/m*)	
P (GPa)	0	31	40	33	0
$N(E_f)$ [states/eV per electron]	0.084	0.064	0.038	0.039	0.044
λ	0.73[a]	0.38	0.33	0.32	0.39
$\langle\omega_{log}\rangle$ (K)	719[a]	811	843	784	749
T_c (K)	27.6[a]	2.5	1.0	0.7	2.8

[a] T_c of MgB_2 is calculated for comparison with other compounds. Note that T_c values in this table are calculated without anharmonicity, using isotropic Eliashberg formalism. T_c for MgB_2 is in agreement with ref. 9. Higher T_c are expected if anisotropy of the electron–phonon interaction is included, *e.g.*, account for anisotropy results in the overestimation of the T_c of MgB_2 to 55 K. On the other hand, anharmonicity of the phonons usually lowers the T_c and in the MgB_2 case, it lowers the T_c to 39 K.[9]

AlB_2-type structure, which is a single-layered phase of this type). The extra layer is located 1.7 Å from the first layer and displaced by 0.8 Å (Aαβ Aαβ…, A represents Mg and α, β are B layers). At 36 GPa, some boron blocks were formed with a pattern of 1 and 2 magnesium atoms per block. Finally, at a higher pressure of 60 GPa, the body-centered tetragonal $BaAl_4$-type structure (space group *I4/mmm*), which is widely adopted among AB_4 intermetallic compounds, forms. In the *I4/mmm* structure, magnesium is located at the center of the truncated rectangular prisms made of boron atoms. This structure is similar to *Cmcm*-MgB_3, in which, there are two magnesium atoms located in each of the truncated rectangular prisms (see Fig. 3(b) and 5(a)).

MgB_6

Although MgB_6 is predicted to be stable with respect to decomposition to the elements (Mg and B),[48] it is not stable against decomposition into elemental boron and MgB_4 (see Fig. 1(a) and (b)). Furthermore, in an experimental study at ambient pressure, MgB_6 was not found as an individual phase.[49]

Since intercalated graphite AC_6 (A = Mg, Ca, Sr, Ba)[50–52] is superconducting, we searched for the lowest enthalpy MgB_6 phases. We observed a hexagonal distorted triple-layered phase, which is the lowest in enthalpy, in the pressure range 15–28 GPa that intrigued us. MgB_6 forms a recently predicted phase at ambient pressure and remains in this *Cmcm* structure up to 15 GPa,[48] above which a triple-layered structure has the lowest enthalpy up to 28 GPa (Fig. 6(c) and (d)). Between 28 GPa and 88 GPa, the $R\bar{3}m$ structure becomes more favorable, and eventually, very high pressure imposes a pattern similar to *I4/mmm*-MgB_4 into $P2_1/m$-MgB_6 (see Fig. 6(a)); this pattern emerges at the pressures greater than 90 GPa in both MgB_6 and MgB_4. We found the *Cmcm* structure to be a semiconductor in agreement with the previous report,[48] whereas the rest of the phases are metallic. The semiconductor–metal transition *Cmcm* → $P2_1/c$ occurs at 15 GPa.

Mg_3B_{10}

Mg_3B_{10}, a boron-rich compound, stable above 55 GPa, has a monoclinic (space group *C2/m*) phase. Above 83 GPa this phase transforms into the *P2/m* phase (Fig. 1(b)). Metastable *Amm2*-Mg_3B_{10}, which we predict to have the lowest enthalpy among Mg_3B_{10} phases in the pressure range 30–42 GPa, has a layered sandwich structure and is superconducting (Fig. 7(c) and (d)).

Superconductivity

Kolmogorov *et al.* proposed metal sandwiches consisting of one or more layers of metal and a graphene-like layer of boron, *i.e.*,

Table 2 Optimized structures of MgB_3

Phase	Lattice parameters	Atom	*x*	*y*	*z*
C2/m [2 f.u.] layered at 30 GPa	*a* = 2.998 Å	Mg(4i)	0.7471	0.0000	0.7982
	b = 5.109 Å	B_1(4g)	0.0000	0.6673	0.0000
	c = 8.852 Å	B_2(8i)	0.5210	0.6717	0.4055
	β = 115.30°				
C2/m [4 f.u.] at 50 GPa	*a* = 7.959 Å	Mg_1(4i)	0.4363	0.0000	0.7000
	b = 2.850 Å	Mg_2(2c)	0.0000	0.0000	0.5000
	c = 10.833 Å	Mg_3(2b)	0.0000	0.5000	0.0000
	β = 116.98°	B_1(4i)	0.9041	0.0000	0.1214
		B_2(4i)	0.8063	0.0000	0.2382
		B_3(4i)	0.7390	0.0000	0.5339
		B_4(4i)	0.6943	0.0000	0.6689
		B_5(4i)	0.8529	0.0000	0.8334
		B_6(4i)	0.7445	0.0000	0.9430
Cmcm [2 f.u.] at 200 GPa	*a* = 2.676 Å	Mg(4c)	0.0000	0.5997	0.2500
	b = 11.521 Å	B_1(4c)	0.0000	0.2490	0.2500
	c = 2.668 Å	B_2(4c)	0.0000	0.8302	0.2500
		B_3(4c)	0.0000	0.9667	0.2500

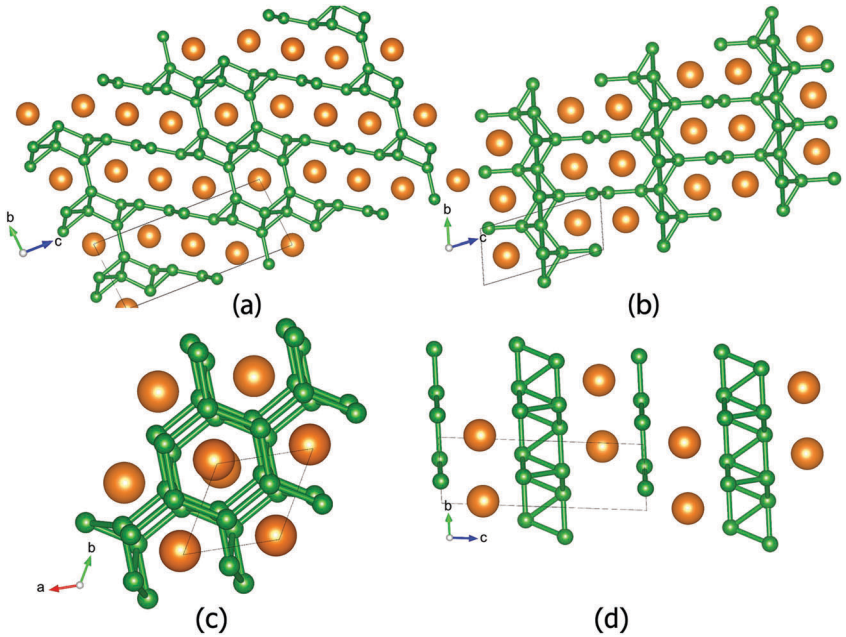

Fig. 3 Structures of thermodynamically stable/metastable phases of MgB_3 (a) $C2/m$ and (b) $Cmcm$ and (c) projections of the layered structure with the space group $C2/m$ along the [001] and (d) [100] directions.

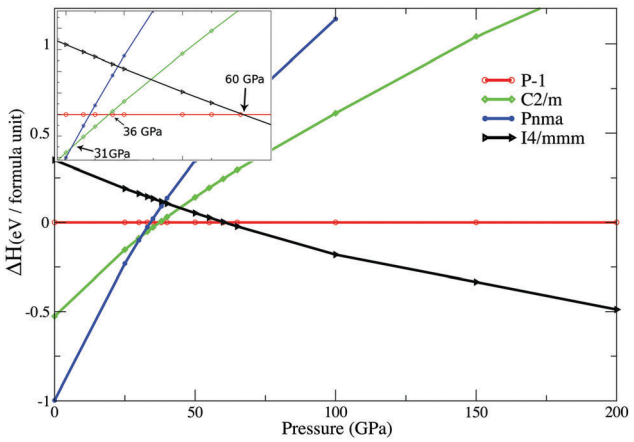

Fig. 4 Enthalpy per formula unit relative to the $P\bar{1}$ structure as a function of pressure for the best phases with the MgB_4 stoichiometry.

MS-2 and MS-4 with a single hexagonal layer of B.[53] In our study we found, boron sandwiches, new structures with one layer of metal atoms alternating with multiple boron layers. Interestingly, boron sandwich structures are ubiquitous here. For example, in MgB_3, there is a layered structure with the space group $C2/m$ below 43 GPa (see Fig. 9.) featuring the αAβγB... stacking of B–Mg layers (A and B denotes Mg and αβγ are B layers). The $C2/m$ structure of MgB_4 in 31–36 GPa, the $Amm2$ structure of Mg_3B_{10} in 30–42 GPa and $P2_1/c$ structure of MgB_6 in 15–28 GPa (see colored areas in Fig. 1(b)) also feature boron sandwiches.

Boron sandwiches are layered structures with stackings of $[MgB_2]$ and/or $[MgB_4]$ blocks (see Fig. 9). For example, Mg_3B_{10} can be represented as a $[MgB_2][MgB_4][MgB_4]$... sequence of layers, and MgB_3 can be represented as $[MgB_2][MgB_4]$.... Superconductivity in MgB_2 is mostly related to the boron layers, *i.e.* B–B σ and π-bonded networks; therefore, sandwich borides with hexagonal boron layers might have superconducting properties. We checked this by electron–phonon coupling calculations. Eliashberg spectral function (α^2F) calculations lead to the results depicted in Fig. 10 and listed in Table 1. The electron–phonon coupling constants (λ) for different structures at given pressures, logarithmic averaged phonon frequencies (ω_{log}) and superconducting transition temperatures (T_c) are also provided (for more information, see the ESI†). The density of states at E_f listed in Table 1 shows that T_c is higher for boron sandwiches with higher $N(E_f)$ per electron. One can see from the projected density of states that 2p states of B atoms, located in planar nets, dominate the DOS at the Fermi level (see Fig. 8. Band structures and the total DOS of other sandwich borides are also provided in the ESI,† Fig. S3, S6 and S10).

The critical temperature of superconductivity is estimated from the Allen–Dynes modified McMillan equation:[54]

$$T_c = \frac{\langle\omega_{log}\rangle}{1.2}\exp\left(\frac{-1.04(1+\lambda)}{\lambda-\mu^*(1+0.62\lambda)}\right), \quad (1)$$

where ω_{log} is the logarithmic average phonon frequency and μ^* is the Coulomb pseudopotential,

$$\omega_{log} = \exp\left[\frac{2}{\lambda}\int\frac{d\omega}{\omega}\alpha^2F(\omega)\ln(\omega)\right] \quad (2)$$

The EPC parameter λ is defined as an integral involving the spectral function α^2F:

$$\lambda = 2\int_0^\infty \frac{\alpha^2F(\omega)}{\omega}d\omega. \quad (3)$$

Here we used μ^* = 0.10 for Coulomb's pseudopotential, as a reasonable value for most materials.[55–57] After MgB_2,

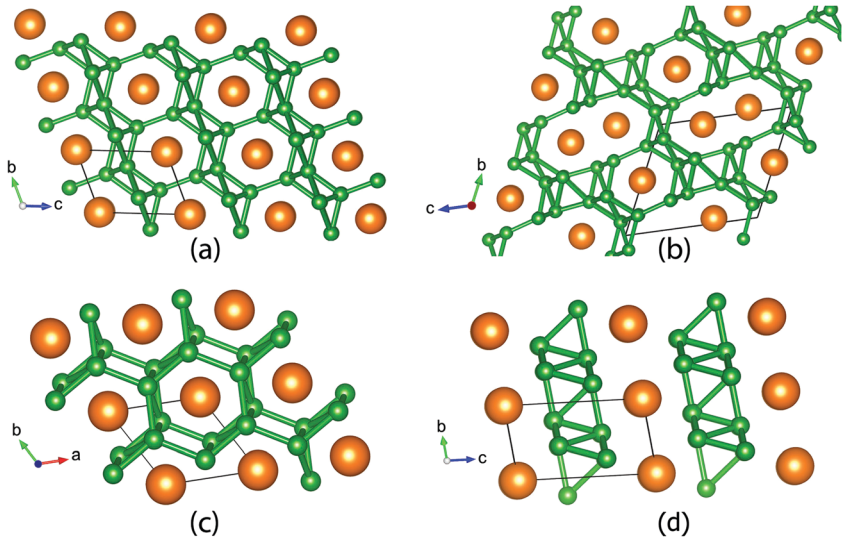

Fig. 5 Structure of MgB_4 phases (a) $I4/mmm$ (b) $P\bar{1}$ and projections of the $C2/m$ structure (c) along the [001] and (d) [100] directions.

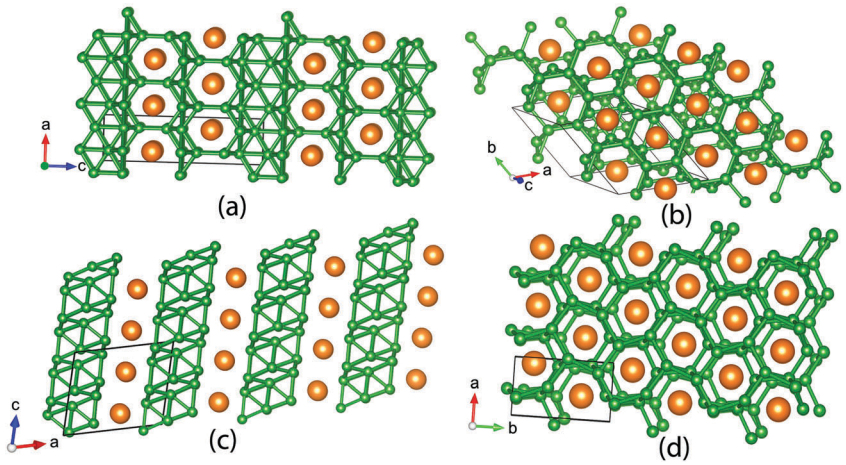

Fig. 6 Structure of magnesium hexaboride phases (a) $P2_1/m$ (b) $R\bar{3}m$ and projections of $P2_1/c$ structure (c) along the [010] and (d) [001] directions. Large spheres are Mg atoms and small spheres are boron atoms.

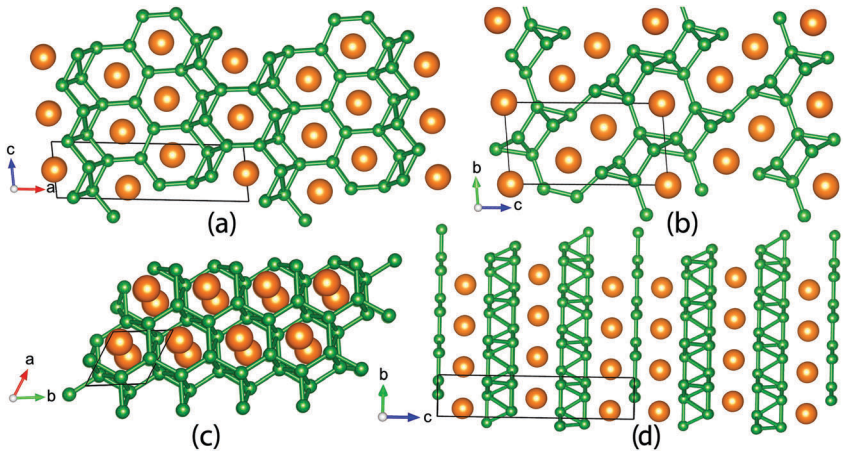

Fig. 7 Structure of Mg_3B_{10} phases (a) $P2/m$, (b) $C2/m$ and projections of $Amm2$ structure (c) along the [001] and (d) [100] directions.

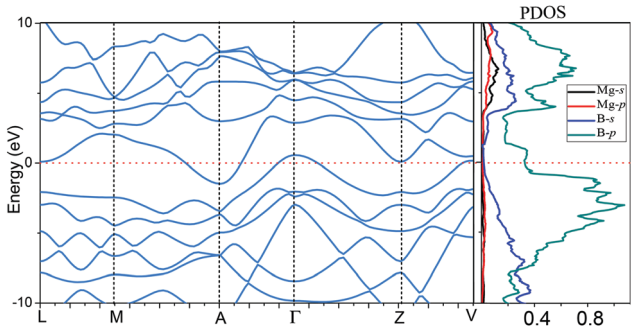

Fig. 8 Band structure and partial densities of states for the $C2/m$-MgB_4 structure at ambient pressure.

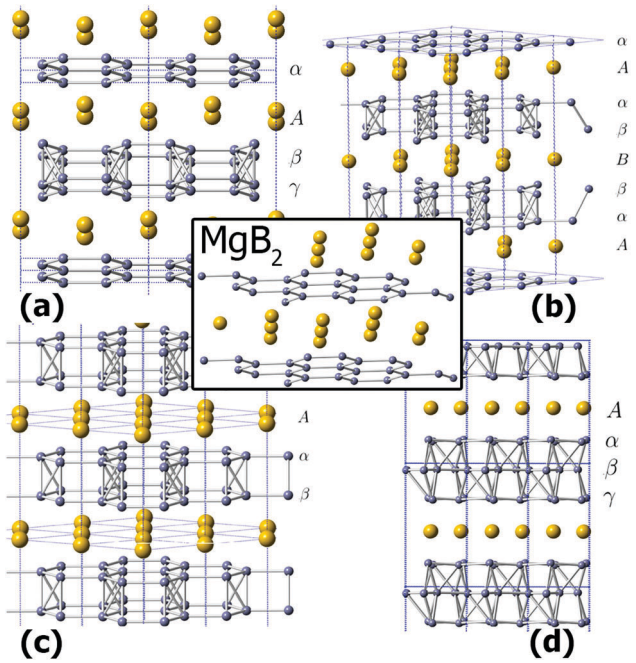

Fig. 9 Boron sandwiches in Mg–B compounds. (a) $C2/m$-MgB_3, (b) $Amm2$-Mg_3B_{10} (c) $C2/m$-MgB_4 and (d) $P2_1/c$-MgB_6.

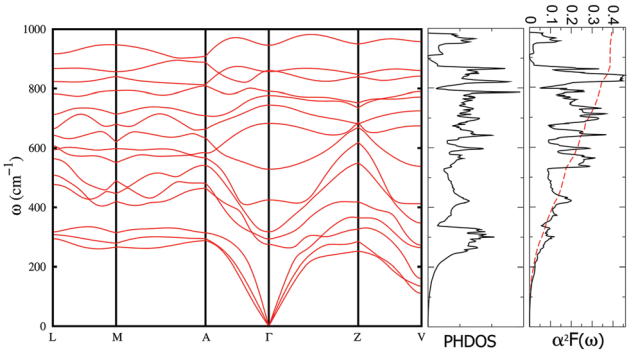

Fig. 10 Phonon band structure, Eliashberg spectral function $\alpha^2F(\omega)$, the integrated electron–phonon coupling constant $\lambda(\omega)$ and PHDOS of $C2/m$-MgB_4 quenched to atmospheric pressure.

$C2/m$-MgB_4 has the highest T_c of 2.8 K at zero pressure (it is metastable at 0 GPa). In $C2/m$-MgB_4, high-frequency phonons, mostly by boron atoms, contribute 80.5% to the total EPC parameter, and low-frequency modes are mainly from magnesium vibrations with 19.5% contribution. Sandwich borides, in general, have a high phonon density between 200 and 400 cm^{-1}; however, the Eliashberg spectral function indicates a poor electron–phonon coupling in this range. Logarithmic average phonon frequencies $\langle\omega_{log}\rangle$ are comparable to those of $P6/mmm$-MgB_2; however, much weaker electron–phonon coupling and lower densities of states at the Fermi level result in very low transition temperatures 0.7–2.8 K. (For more information about phonon band structures, phonon density of states, Eliashberg spectral function and electronic band structures of these phases, see the ESI.†)

Directly relevant to superconductivity of sandwich borides is the value of DOS at the Fermi level. For example, the DOS is 0.044 states/eV per electron for $C2/m$-MgB_4. This is about half the value of MgB_2 which is 0.084 states/eV per electron. We can see a trend of increasing T_c when we have higher DOS (values are listed in Table 1). However, other parameters are also essential. Since logarithmic average phonon frequencies are almost equal, outstanding MgB_2 superconductivity can be related to the higher density of states at the E_f mainly from boron p-states and a stronger electron–phonon coupling parameter λ = 0.73 mainly affected by lower frequency modes. λ of other boron sandwiches is about half of the value of MgB_2 (see values listed in Table 1), which due to exponential dependence of T_c on λ, the T_c value of MgB_2 is about 10 times higher than other magnesium borides.

Conclusions

Using the *ab initio* evolutionary structure search, we have extended our previous study of MgB_2 to other possible Mg–B compounds up to megabar pressures. A remarkable variety of candidate high-pressure ground states has been identified. In this systematic study, under pressures from 0 to 200 GPa, we have found 6 stable compounds, *i.e.*, MgB_2, MgB_3, MgB_4, Mg_3B_{10}, MgB_7 and MgB_{12}. Interestingly, MgB_7 and MgB_{12}, which are reported to be stable at ambient pressure, are not competitive at very high (above 90 GPa) pressure. In all compounds, at sufficiently high pressures sandwich borides give way to structures with three-dimensional topology.

Most of the predicted stable phases are metallic. No magnesium-rich phases are stable. By decreasing the pressure to 0 GPa, the T_c value of $C2/m$-MgB_4 is enhanced and reaches 2.8 K. The importance of layered structures at the boron-rich end of the Mg–B phase diagram is noteworthy. The valence bands close to and below the E_f are dominated by boron p-states in layered structures. Therefore, EPC calculations are performed and revealed that Mg–B sandwich borides are superconducting with the T_c of 2.5, 1.0 and 0.7 K for $C2/m$-MgB_3, $Amm2$-Mg_3B_{10} and $C2/m$-MgB_4 at 31, 40 and 33 GPa, respectively.

Acknowledgements

We thank DARPA (grant W31P4Q1210008), the Government of Russian Federation (14.A12.31.0003) and the Foreign Talents

Introduction and Academic Exchange Program (B08040). X. F. Z. thanks the National Science Foundation of China (grant no. 11174152), the National 973 Program of China (grant no. 2012CB921900), and the Program for New Century Excellent Talents in University (grant no. NCET-12-0278).

References

1 H. J. Choi, S. G. Louie and M. L. Cohen, *Phys. Rev. B: Condens. Matter Mater. Phys.*, 2009, **80**, 064503.
2 J. K. Dewhurst, S. Sharma, C. Ambrosch-Draxl and B. Johansson, *Phys. Rev. B: Condens. Matter Mater. Phys.*, 2003, **68**, 020504.
3 B. Andrzejewski, *Cryogenics*, 2008, **48**, 478–482.
4 M. J. Mehl, D. A. Papaconstantopoulos and D. J. Singh, *Phys. Rev. B: Condens. Matter Mater. Phys.*, 2001, **64**, 140509.
5 R. J. Cava, H. Takagi, B. Batlogg, H. W. Zandbergen, J. J. Krajewski, W. F. Peck, R. B. van Dover, R. J. Felder, T. Siegrist, K. Mizuhashi, J. O. Lee, H. Eisaki, S. A. Carter and S. Uchida, *Nature*, 1994, **367**, 146–148.
6 J. Nagamatsu, N. Nakagawa, T. Muranaka, Y. Zenitani and J. Akimitsu, *Nature*, 2001, **410**, 63–64.
7 U. Welp, A. Rydh, G. Karapetrov, W. Kwok, G. Crabtree, C. Marcenat, L. Paulius, L. Lyard, T. Klein, J. Marcus, S. Blanchard, P. Samuely, P. Szabo, A. Jansen, K. Kim, C. Jung, H.-S. Lee, B. Kang and S.-I. Lee, *Phys. C*, 2003, **385**, 154–161.
8 A. Goncharov and V. Struzhkin, *Phys. C*, 2003, **385**, 117–130.
9 H. J. Choi, D. Roundy, H. Sun, M. L. Cohen and S. G. Louie, *Phys. Rev. B: Condens. Matter Mater. Phys.*, 2002, **66**, 020513.
10 A. Brinkman, A. A. Golubov, H. Rogalla, O. V. Dolgov, J. Kortus, Y. Kong, O. Jepsen and O. K. Andersen, *Phys. Rev. B: Condens. Matter Mater. Phys.*, 2002, **65**, 180517.
11 I. I. Mazin, O. K. Andersen, O. Jepsen, O. V. Dolgov, J. Kortus, A. A. Golubov, A. B. Kuz'menko and D. van der Marel, *Phys. Rev. Lett.*, 2002, **89**, 107002.
12 D. G. Hinks, H. Claus and J. D. Jorgensen, *Nature*, 2001, **411**, 457–460.
13 R. Ribeiro, S. Bud'ko, C. Petrovic and P. Canfield, *Phys. C*, 2003, **385**, 16–23.
14 J. S. Slusky, N. Rogado, K. A. Regan, M. A. Hayward, P. Khalifah, T. He, K. Inumaru, S. M. Loureiro, M. K. Haas, H. W. Zandbergen and R. J. Cava, *Nature*, 2001, **410**, 343–345.
15 P. Li, G. Gao, Y. Wang and Y. Ma, *J. Phys. Chem. C*, 2010, **114**, 21745–21749.
16 A. R. Oganov, J. Chen, C. Gatti, Y. Ma, Y. Ma, C. W. Glass, Z. Liu, T. Yu, O. O. Kurakevych and V. L. Solozhenko, *Nature*, 2009, **457**, 863–867.
17 T. Tomita, J. J. Hamlin, J. S. Schilling, D. G. Hinks and J. D. Jorgensen, *Phys. Rev. B: Condens. Matter Mater. Phys.*, 2001, **64**, 092505.
18 Y. Ma, Y. Wang and A. R. Oganov, *Phys. Rev. B: Condens. Matter Mater. Phys.*, 2009, **79**, 054101.
19 M. Yaknc, Y. Balc, M. Aksan, H. Adigüzel and A. Gencer, *J. Supercond.*, 2002, **15**, 607–611.
20 A. Pediaditakis, M. Schroeder, V. Sagawe, T. Ludwig and H. Hillebrecht, *Inorg. Chem.*, 2010, **49**, 10882–10893.
21 S. Shah and A. N. Kolmogorov, *Phys. Rev. B: Condens. Matter Mater. Phys.*, 2013, **88**, 014107.
22 A. Hermann, A. McSorley, N. W. Ashcroft and R. Hoffmann, *J. Am. Chem. Soc.*, 2012, **134**, 18606–18618.
23 A. V. D. Geest and A. Kolmogorov, *CALPHAD: Comput. Coupling Phase Diagrams Thermochem.*, 2014, **46**, 184–204.
24 A. R. Oganov and C. W. Glass, *J. Chem. Phys.*, 2006, **124**, 244704.
25 A. R. Oganov, Y. Ma, A. O. Lyakhov, M. Valle and C. Gatti, *Rev. Mineral. Geochem.*, 2010, **71**, 271–298.
26 A. R. Oganov, A. O. Lyakhov and M. Valle, *Acc. Chem. Res.*, 2011, **44**, 227–237.
27 Q. Zhu, A. R. Oganov, C. W. Glass and H. T. Stokes, *Acta Crystallogr., Sect. B: Struct. Sci.*, 2012, **68**, 215–226.
28 W. Zhang, A. R. Oganov, A. F. Goncharov, Q. Zhu, S. E. Boulfelfel, A. O. Lyakhov, E. Stavrou, M. Somayazulu, V. B. Prakapenka and Z. Konôpková, *Science*, 2013, **342**, 1502–1505.
29 X. Dong, A. R. Oganov, A. F. Goncharov, E. Stavrou, S. Lobanov, G. Saleh, G.-R. Qian, Q. Zhu, C. Gatti and V. L. Deringer, *et al.*, *Nat. Chem.*, 2017, **9**, 440–445.
30 M. M. D. Esfahani, Z. Wang, A. R. Oganov, H. Dong, Q. Zhu, S. Wang, M. S. Rakitin and X.-F. Zhou, *Sci. Rep.*, 2016, **6**, 22873.
31 M. M. D. Esfahani, A. R. Oganov, H. Niu and J. Zhang, *Phys. Rev. B*, 2017, **95**, 134506.
32 A. O. Lyakhov, A. R. Oganov, H. T. Stokes and Q. Zhu, *Comput. Phys. Commun.*, 2013, **184**, 1172–1182.
33 G. Kresse and J. Furthmüller, *Phys. Rev. B: Condens. Matter Mater. Phys.*, 1996, **54**, 11169–11186.
34 J. P. Perdew, K. Burke and M. Ernzerhof, *Phys. Rev. Lett.*, 1996, **77**, 3865–3868.
35 P. E. Blöchl, *Phys. Rev. B: Condens. Matter Mater. Phys.*, 1994, **50**, 17953–17979.
36 H. J. Monkhorst and J. D. Pack, *Phys. Rev. B: Solid State*, 1976, **13**, 5188–5192.
37 P. Giannozzi, S. Baroni, N. Bonini, M. Calandra, R. Car, C. Cavazzoni, D. Ceresoli, G. L. Chiarotti, M. Cococcioni, I. Dabo, A. Dal Corso, S. de Gironcoli, S. Fabris, G. Fratesi, R. Gebauer, U. Gerstmann, C. Gougoussis, A. Kokalj, M. Lazzeri, L. Martin-Samos, N. Marzari, F. Mauri, R. Mazzarello, S. Paolini, A. Pasquarello, L. Paulatto, C. Sbraccia, S. Scandolo, G. Sclauzero, A. P. Seitsonen, A. Smogunov, P. Umari and R. M. Wentzcovitch, *J. Phys.: Condens. Matter*, 2009, **21**, 395502.
38 S. Souma, H. Komoda, Y. Iida, T. Sato, T. Takahashi and S. Kunii, *J. Electron. Spectrosc. Relat. Phenom.*, 2005, **147**, 503–506.
39 S. Li, O. Prabhakar, T. T. Tan, C. Q. Sun, X. L. Wang, S. Soltanian, J. Horvat and S. X. Dou, *Appl. Phys. Lett.*, 2002, **81**, 874–876.
40 Y. Liang, Y. Gou, X. Yuan, Z. Zhong and W. Zhang, *Chem. Phys. Lett.*, 2013, **580**, 48–52.
41 H. Niu, X.-Q. Chen, W. Ren, Q. Zhu, A. R. Oganov, D. Li and Y. Li, *Phys. Chem. Chem. Phys.*, 2014, **16**, 15866–15873.
42 S. C. Yan, G. Yan, C. F. Liu, Y. F. Lu and L. Zhou, *J. Am. Ceram. Soc.*, 2007, **90**, 2184–2188.
43 X. Meng, K. Bao, P. Zhu, Z. He, Q. Tao, J. Li, Z. Mao and T. Cui, *J. Appl. Phys.*, 2012, **111**, 1–6.
44 H. Niu, J. Wang, X.-Q. Chen, D. Li, Y. Li, P. Lazar, R. Podloucky and A. N. Kolmogorov, *Phys. Rev. B: Condens. Matter Mater. Phys.*, 2012, **85**, 144116.

45 M. B. Yahia, O. Reckeweg, R. Gautier, J. Bauer, T. Schleid, J. F. Halet and J. Y. Saillard, *Inorg. Chem.*, 2008, **47**, 6137–6143.
46 Z. Liu, X. Han, D. Yu, Y. Sun, B. Xu, X. F. Zhou, J. He, H. T. Wang and Y. Tian, *Appl. Phys. Lett.*, 2010, **96**, 4–7.
47 G. Bruzzone, *Acta Crystallogr., Sect. B: Struct. Crystallogr. Cryst. Chem.*, 1969, **25**, 1206–1207.
48 H. Wang, K. A. LeBlanc, B. Gao and Y. Yao, *J. Chem. Phys.*, 2014, **140**, 044710.
49 G. Moiseev and A. Ivanovskii, *Inorg. Mater.*, 2005, **41**, 1061–1066.
50 M. Calandra and F. Mauri, *Phys. Rev. B: Condens. Matter Mater. Phys.*, 2006, **74**, 094507.
51 Z.-H. Pan, J. Camacho, M. H. Upton, A. V. Fedorov, C. A. Howard, M. Ellerby and T. Valla, *Phys. Rev. Lett.*, 2011, **106**, 187002.
52 J. S. Kim, L. Boeri, R. K. Kremer and F. S. Razavi, *Phys. Rev. B: Condens. Matter Mater. Phys.*, 2006, **74**, 214513.
53 A. N. Kolmogorov and S. Curtarolo, *Phys. Rev. B: Condens. Matter Mater. Phys.*, 2006, **74**, 224507.
54 P. B. Allen and R. C. Dynes, *Phys. Rev. B: Solid State*, 1975, **12**, 905–922.
55 C. F. Richardson and N. W. Ashcroft, *Phys. Rev. Lett.*, 1997, **78**, 118–121.
56 Y. Xie, A. R. Oganov and Y. Ma, *Phys. Rev. Lett.*, 2010, **104**, 177005.
57 X.-F. Zhou, A. R. Oganov, X. Dong, L. Zhang, Y. Tian and H.-T. Wang, *Phys. Rev. B: Condens. Matter Mater. Phys.*, 2011, **84**, 054543.

